



# Analysis Method of High-Field Pinning Centers in NbTi Wires and MgB<sub>2</sub> Wires

Daniel Gajda<sup>1</sup>

Received: 10 July 2018 / Accepted: 3 October 2018 / Published online: 9 October 2018  
© The Author(s) 2018

## Abstract

The main purpose of this article is to show an easier and more accurate method for analyzing high-field pinning centers. Previous methods did not allow for precise analysis and research on high-field pinning centers, they studied only the dominant pinning mechanism, and they required a maximum of pinning force ( $F_{pmax}$ ) to analyze pinning centers. The main advantage of this method can be used in samples without the maximum pinning force required by other methods to analyze the pinning mechanism. In addition, this method allows us to observe even small changes in the density of individual pinning centers. This method is based on analysis of critical current density values in different ranges of reduced magnetic field. The method of analysis of high-field pinning centers allows primarily to develop methods and directions for creation of high-field pinning centers. The surface pinning centers are strong pinning centers in low magnetic fields and very weak pinning centers in middle and high magnetic fields. Additionally, the analysis of pinning centers shows that dislocations, strains, substitutions in the crystal lattice, and precipitation inside the grains create strong pinning centers in high magnetic fields and very weak pinning centers in low and middle magnetic fields. Research indicates that strains, substitutions in the crystal lattice, and precipitates inside grains form pinning centers that operate in the high magnetic field range.

**Keywords** Analysis method of pinning centers · Dominant pinning mechanism · NbTi wires · MgB<sub>2</sub> wires

---

✉ Daniel Gajda  
dangajda@op.pl; d.gajda@intibs.pl

<sup>1</sup> Institute of Low Temperature and Structure Research, Polish Academy of Sciences, Okólna 2, 50-422 Wrocław, Poland

## 1 Introduction

In type II superconducting materials, pinning of vortices (magnetic flux) occurs [1]. The transport current and the magnetic flux in the superconductor material introduce the Lorentz force which acts on the vortex. Movement of the vortices generates a voltage. In a superconducting material without defects, the critical current density is zero. The movement of the vortex can be stopped, however, by means of pinning centers. Vortex cores with a diameter of  $2\xi$  (where  $\xi$  is the coherence length) in the normal state will increase the energy of the system. This energy can be reduced by the change in Gibbs free energy,  $\Delta G$  (where  $\Delta G = nU_v - BH$ , with  $n$  the number of vortices and  $U_v$  the energy of the vortex magnetic field), when the core of the vortex is placed at a normal area (pinning center) [1]. Pinning centers can be defects in the form of voids, precipitates, grain boundaries, and dislocations [2].

Currently, we have several models which describe the anchorage of vortex lattice on different types of pinning centers. The first models describing the interaction of flux line lattice with pinning centers were presented by Kramer [3, 4]. Next, a model was presented by Dew-Hughes in 1974 [5]. Dew-Hughes [5] proposed several patterns for determining the dominant types of pinning centers in superconducting material. These formulas describe changes of the dominant pinning mechanism in the magnetic field. A similar model was also presented by Higuchi et al. [6]. It also describes changes in the dominant pinning mechanism in a magnetic field. Studies on the pinning model were also conducted by Evetts and Plummer [7], Fietz and Webb [8], Hampshire and Taylor [9], Key and Hampshire [10], and Ekin [11]. The pinning mechanism can also be examined by analyzing  $\delta l$  and  $\delta T_c$ . The  $\delta l$  pinning mechanism is connected with charge carrier mean free path variations, and the  $\delta T_c$  pinning mechanism is associated with randomly distributed spatial variations in the transition temperature [12, 13]. Ghorbani et al. [13] showed that the  $\delta l$  pinning mechanism is dominant at low temperature and the  $\delta T_c$  pinning mechanism is dominant at high temperature. Matsushita indicates that based on the analysis Kramer can be concluded that there are two types of high-field pinning centers dependent on the strength of pinning [14]. Blatter et al. [1], Kwok et al. [15], and Thomann et al. [16] also conducted research and theoretical analysis on strong pinning centers in high-temperature superconductor materials. Blatter et al. [1] suggested that the most prominent type of strong pinning to date is pinning by columnar defects. Kwok et al. [15] indicated that irradiation defects only improve pinning at high magnetic fields and not at very high temperatures. Thomann et al. [16] showed that strong pinning is dependent on dynamics of the vortex lattice. Klaassen et al. [17] also indicated linear defects create strong pinning centers.

Pinning centers can be categorized in terms of the interaction between the vortex and the defect, e.g., attractive or repulsive, and their location in the structure [18]. Livingston [2] indicates that there are different types of pinning centers volume, surface, and point centers (e.g., precipitates and voids close to the coherence length). These pinning centers are most effective for increasing critical current density in low and medium magnetic fields [18–20]. In addition, Gajda et al. [21] showed that these pinning centers in  $\text{MgB}_2$  increase the critical current density ( $J_c$ ) above 30 K, whereas pinning centers created by dislocations (line pinning centers) [2], substitution of C for B (lattice substitution pinning centers) [22], and precipitates inside the grain (inside

grains pinning centers) [23] very effectively increase the  $J_c$  in high magnetic fields [18]. These pinning centers also significantly increase  $J_c$  from 4.2 to 30 K and decrease  $J_c$  above 30 K in  $\text{MgB}_2$  [21]. Gajda et al. [18] suggested that precipitates inside grains in NbTi do not reduce the critical parameters: the superconducting critical temperature ( $T_c$ ), the irreversible magnetic field ( $B_{irr}$ ), and the upper critical field ( $B_{c2}$ ) of NbTi grains, and they effectively increase  $J_c$  in magnetic fields above 9.5 T. Previous results suggest that the dislocations and substitution into the lattice (e.g., in  $\text{MgB}_2$  material, the substitution of C for B) create pinning centers, which operate in the same high magnetic fields. Gajda et al. [18] showed for the first time that dislocations effectively increase  $J_c$  in magnetic fields from 6 to 8 T in NbTi. There are several methods that allow us to obtain high-field pinning centers and more connections between the grains in superconducting wires, tapes, bulks, and thin layers, e.g., cold drawing (CD) [20, 24–26], equal-channel multi-angle pressing (ECMAP) [27, 28], cold rolling (CR) [25, 29], cold pressure (CP) [30], hot isostatic pressure (HIP) [25, 31, 32], and C doping [33–36].

## 2 Physical Properties and Pinning Centers in NbTi Wires

The values of critical parameters in NbTi wires depend on the microstructure of the superconducting material. The NbTi material creates two stable phases: the  $\beta$  (NbTi) phase and the  $\alpha$  phase (Ti precipitates between grains), and three metastable phases: the  $\alpha'$  phase (Ti precipitates inside grains), the  $\alpha''$  phase (Ti precipitates between grains), and the  $\omega$  phase [37]. The temperature at which the stable  $\beta$  phase is formed is dependent on the ratio of Nb to Ti. The small difference in size 2% between the atoms of Ti and Nb causes the formation of a crystal lattice with the body-centered cubic (BCC) structure with a lattice constant of about 0.3285 nm [37–39]. The Ti precipitates between the grains are created during the heating of the NbTi material in the temperature [37]. The stable  $\alpha$ -Ti phase has a hexagonal close-packed structure [37] and lattice constants  $a = 0.2956$  nm and  $c = 0.4716$  nm. The  $\alpha$ -Ti phase also contains a small amount of Nb from 1 to 2% [37]. The low content of Nb causes the Ti precipitates between the grains to have a very low critical temperature of about 0.39 K [40].

The formation rate of Ti precipitates between grains is dependent on the Ti content in the NbTi material [41], the density of crystal dislocations [4, 42, 43], size and number of the voids [40, 44], the shapes of the NbTi grains, the heating temperature, and amount of the metastable phases [45]. After annealing, the Ti precipitates between grains have thickness of 100–200 nm [41–48]. Lee suggests that a large number of Ti precipitates between grains (about 10%) are produced during the first heating process [37]. The thickness of these precipitates is decreased by using cold working for NbTi wires. The cold drawing allows us to obtain Ti precipitates between grains with a thickness of 1–5 nm [41–43, 46–49]. Additionally, the cold drawing increases the length of the Ti precipitates between grains from 50–100 nm to 1–10  $\mu\text{m}$  [38]. The shapes, locations, and directions of Ti precipitates between grains also affect the critical current density of the wires [50]. The highest critical current density in NbTi wires was obtained for a content of Ti precipitates between grains in the range from 25 to

33% [41, 51]. Currently, at the temperature of liquid helium and magnetic field of 5 T, the highest critical current density that has been obtained is  $5400 \text{ A/mm}^2$  [51]. Theoretical calculations show that in NbTi wires it might be possible to obtain the critical current density of  $18,000 \text{ A/mm}^2$  (5 T and 4.2 K) [52]. Lee and Larbalestier [44] demonstrated that the highest pinning force can be obtained for Ti precipitates between grains with a thickness of about 1 nm and a separation distance of about 4 nm. Cold drawing in NbTi wires creates dislocations. Panek et al. [19] and Matsushita and Kupfer [20] demonstrated that dislocations form high-field pinning centers.

NbTi material has the critical temperature of about 9.6 K and an irreversible magnetic field of about 11.5 T [37, 38, 47]. The resistivity of the NbTi material in the normal state is dependent on the content of Ti in the NbTi material [52].

The NbTi material has three martensitic phases, e.g.,  $\alpha'$ ,  $\alpha''$ , and  $\omega$  [53]. These phases are formed during fast cooling of NbTi material. The  $\alpha''$  (C-face centered orthorhombic) and  $\omega$  [hexagonal close-packed (HCP)] phases are precipitates between grains [53–56]. These precipitations can create surface and point pinning centers. The NbTi material also has Ti precipitates inside the grains ( $\alpha'$ —Widmanstätten Ti). This phase has needle-shaped grains and structure of the HCP type [53]. This phase is created in NbTi compounds with 13 wt% Nb [53] and NbTi compounds with Nb+53 wt% Ti [23, 37]. The results suggest that these Ti precipitates act as pinning centers in very high magnetic fields (near  $B_{\text{irr}}$ ) [18]. This is very important because it allows us to understand why the critical current density is low near  $B_{\text{irr}}$ . The magnetic and non-magnetic particles decrease  $J_c$  in NbTi wires in high magnetic fields [57–60].

### 3 Physical Properties and Pinning Centers in MgB<sub>2</sub> Wires

The superconductivity of MgB<sub>2</sub> was discovered at 2001 by the research group of Prof. Akimitsu [61]. It is an intermetallic compound with hexagonal structure of  $p6/mmm$  and lattice constants  $a = 3.086 \text{ \AA}$  and  $c = 3.524 \text{ \AA}$  [61]. MgB<sub>2</sub> has low density of  $2.6 \text{ g/cm}^3$  [62], low anisotropy in the range of 1.5–5 [62, 63], and high critical temperature of 39 K [61]. This superconductor has coherence length of  $\xi = 5 \text{ nm}$  [62, 63] and very low resistivity [33, 62]. Penetration depth is in the range from 100 to 140 nm [64], and the Ginzburg–Landau parameter is about 26 [62]. The irreversible magnetic field ( $B_{\text{irr}}$ ) is about 22 T, and the lower critical field ( $H_{c1}$ ) is in the range from 27 to 48 mT [64]. This material possesses two superconducting gaps [65].

The annealing temperature for in situ MgB<sub>2</sub> wires is determined on the basis of the phase diagram [66]. The phase diagram indicates that there is a large difference in melting point between Mg (650 °C) and B (2100 °C). Liu et al. [66] showed that too high annealing temperature and high boron content lead to creation of MgB<sub>4</sub> and MgB<sub>7</sub> phases, which are not superconducting. The large number and big size of the grains of MgB<sub>4</sub> and MgB<sub>7</sub> phases diminish the quantity of superconducting phase and decrease the critical current density ( $J_c$ ) of the MgB<sub>2</sub> wires. It was shown that annealing Mg and B in the solid state (below 650 °C) allows us to obtain small grains. Mustapic et al. [67] showed that the largest amount of MgB<sub>2</sub> phase is obtained at an annealing temperature of 570 °C. The small grains allow abundant connections between grains in MgB<sub>2</sub> wires. MgB<sub>2</sub> material has a significant disadvantage due

to shrinkage. This effect creates large voids that reduce the number of connections between the grains in in situ MgB<sub>2</sub> wires. Jung et al. [68] showed that the volume of the MgB<sub>2</sub> material can be reduced by up to 25% in in situ MgB<sub>2</sub> wires.

In superconducting wires, the critical current density ( $J_c$ ) depends on the number of pinning centers and the number of connections between the grains. Undoped MgB<sub>2</sub> wires have very small values of critical parameters ( $J_c$ ,  $H_{irr}$ , and  $H_{c2}$ ) in high magnetic fields, because this material has only a small amount of high-field pinning centers. Research has shown that high-field pinning centers in MgB<sub>2</sub> wires can result from substitution of C for B and dislocations [32, 33, 68, 69]. Hot isostatic pressing (HIP) significantly increases the number of high-field pinning centers, e.g., increase in the density of dislocations, and accelerates the substitution of C for B, allowing to obtain a uniform distribution of pinning centers [27, 31, 35, 36]. In addition, results indicate that using boron grains with nanosizes makes it possible to obtain more high-field pinning centers than usage of large particles of boron [70, 71]. Studies also showed that high isostatic pressure increases the number of connections between the grains densifying material [31, 36]. Transport and magnetic measurements have demonstrated that high-field pinning centers (dislocations and strains) significantly increase  $J_c$  from 4.2 to 30 K and decrease  $J_c$  above 30 K [21, 36, 72].

The low- and middle-field pinning centers in MgB<sub>2</sub> wires are formed by surface and point pinning centers. The surface pinning centers are large precipitates (e.g., MgB<sub>4</sub> and MgB<sub>7</sub>), impurities (MgO), and voids [2, 31, 33, 35, 36]. The point pinning centers are precipitates, impurities, and voids with thickness close to the coherence length [2, 35, 36].

Currently, MgB<sub>2</sub> wires and tapes are prepared by several techniques, e.g., powder-in-tube (PIT) method [73], the internal Mg infiltration process (AIMI) [74], and the formation of thin layers. The highest  $J_c$  values in high magnetic fields are obtained for in situ MgB<sub>2</sub> wires, e.g., undoped MgB<sub>2</sub> wires which have  $J_c$  of 1000 A/mm<sup>2</sup> in 4 T at 4.2 K and 100 A/mm<sup>2</sup> in 6.2 T at 4.2 K [75], and C-doped MgB<sub>2</sub> wire has  $J_c$  of 1000 A/mm<sup>2</sup> in 7 T at 4.2 K [75]. The AIMI process allows to obtain high  $J_c$  in doped MgB<sub>2</sub>, e.g., 800 A/mm<sup>2</sup> in 8 T at 4.2 K [75].

#### 4 Fabrication of NbTi Wires, MgB<sub>2</sub> Wires, and Method of $J_c$ Measurements

A bimetallic rod of Nb + 60 at.% Ti (Nb + 44 wt% Ti) in a copper shield was produced at the A. A. Galkin Donetsk Institute for Physics and Engineering, National Academy of Sciences, Ukraine, using the method of hot pressing (HP) at 750 °C [76]. The NbTi rod had a diameter of 15 mm. One part of the rod 15 mm in diameter was processed by using equal-channel multi-angle pressing (ECMAP), and the second was made without the ECMAP method (Table 1). Three cycles of hydroextrusion (HE) reduced the rod diameter to 3 mm. The next few passes of cold drawing reduced the rod diameter to 0.3 mm [27, 28, 76].

MgB<sub>2</sub> wires were produced at Hyper Tech Research by using a continuous tube forming and filling (CTFF) process [77]. These MgB<sub>2</sub> wires have 6, 18, or 36 filaments and a Nb barrier.

**Table 1** The NbTi wires with a diameter of 0.3 mm

No.	Annealing temperature (°C)	Number of ECMAP cycles
A	750	0
B	750	12

**Table 2** The MgB<sub>2</sub> wires with diameter of 0.83 mm

No.	Doping	Temperature (°C)	Pressure (Pa)	Time (min)	Refs.
C	Undoped	700	0.1 M	15	[31]
D	Undoped	700	1 G	15	[31]
E	10% SiC	700	0.1 M	15	[35]
F	10% SiC	700	1 G	15	[35]
G	10% SiC	700	1.4	15	[35]
H	10% SiC	680	1 G	15	[35]
I	2% C	700	0.1 M	15	[36]
J	2% C	70	1 G	15	[36]

The filaments were composed of nanosized B, pre-doped with 2 at.% C and 10% SiC, with an Mg-to-B ratio of 1:2 and 1.1:2, respectively. The wires were made to a diameter of 0.83 mm, with a fill factor of 15%. All MgB<sub>2</sub> wires were annealed in isostatic pressure at the Institute of High Pressure Research in Warsaw [78–80]. The HIP was conducted in a 5 N argon atmosphere in a gas pressure chamber (Table 2).

Critical current ( $I_c$ ) measurements were taken with the traditional four-probe resistivity method at 4.2 K in two different setups in the Institute of Low Temperature and Structure Research PAS. First, the current was swept while keeping the magnetic field constant. The second setup was the field swept type, where the transport current is kept constant, and the magnetic field is quickly swept. In both cases, the  $I_c$  value was determined using a 1  $\mu\text{V}/\text{cm}$  criterion [81, 82].  $I_c$  at 20 K was measured at the Institute for Solid State and Materials Research, Dresden [29]. The critical temperature measurements and the critical magnetic field measurements were taken using the four-probe resistive method on a physical properties measurement system (PPMS), operating at 100 mA and 15 Hz at the International Institute of Low Temperature and Structure Research PAS [35, 36]. Measurements for each sample were taken several times in different places. The  $T_c$ ,  $B_{\text{irr}}$ , and  $B_{c2}$  were determined on the basis of criteria of 50%, 10%, and 90% of the normal-state resistance.

#### 4.1 Detection of Damaged Barrier

The Nb [77] and ex situ MgB<sub>2</sub> [83] barriers in MgB<sub>2</sub> wires eliminate any reaction of Mg with the sheathing of the wires. This allows us to obtain high  $J_c$  in MgB<sub>2</sub> wires. Scanning electron microscopy (SEM) analysis showed that the Nb and ex situ

MgB<sub>2</sub> barriers sometimes are damaged [81, 84]. Currently, we can detect damage in the barrier by using two transport methods. In the first method, a jump in the electric field in low magnetic fields indicates a break in the Nb and ex situ MgB<sub>2</sub> barriers [85]. In the field sweep method, rapidly increasing magnetic field and constant current are used [85]. Further research allowed for elaboration of the second method, which is simpler and easier to use. In this method, a jump appearance in the resistance at low temperature indicates a break in the Nb and ex situ MgB<sub>2</sub> barriers in MgB<sub>2</sub> wires [81, 84, 86]. In the temperature sweep method, rapidly increasing temperature and constant current are used [81, 84, 86]. In this method, we can test wires using PPMS. This makes it more easily available method. It was also demonstrated that magnetic measurements do not allow detection of damage in the barrier [84]. Further research has shown that this method can also detect the damages of the barrier of iron-based superconducting wires [87]. Damage to the Nb barrier significantly reduces  $J_c$  in high magnetic fields [81]. This greatly limits research on high-field pinning centers. The solution to this problem has made it possible to better understand the formation of high-field pinning centers.

## 5 Analysis of Pinning Centers in NbTi Wires

### 5.1 At 4.2 K

Previous studies indicated only the dominant pinning mechanism in superconductors, e.g., Dew-Hughes [5] and Higuchi et al. [6]. These methods cannot analyze the other types of pinning centers. In addition, these methods for pinning analysis of the dominant pinning mechanism need the maximum pinning force ( $F_{pmax}$ ), which significantly limits their use. The results in Ref. [18] make it possible to analyze different types of pinning centers in different magnetic fields. This method complements the methods of Dew-Hughes [5] and Higuchi et al. [6] and allows for better analysis of high-field pinning centers in undoped and doped MgB<sub>2</sub> wires. The main advantage of this method is that we do not need  $F_{pmax}$  for analysis of pinning centers. Another advantage of this method is the possibility of analyzing all types of pinning centers that were created in the superconducting material. This is very important because it allows us to obtain high  $J_c$  in superconducting wires in selected magnetic fields (in which the wire will be used).

The study in Ref. [18] shows that in samples A and B we do not have Ti precipitates (and thus a lack of point pinning centers). From results for sample A (Fig. 1a), in the range of reduced magnetic field  $B/B_{irr}$  from 0 to 0.3, we see that  $J_c$  is decreased by one order of magnitude. This indicates that the surface pinning is very weak. This rapid decrease is also due to the lack of point pinning centers. In the range from 0.3 to 0.45, we see a further decrease in  $J_c$  by 20%. On the other hand, in the range from 0.45 to 0.5, one can see that  $J_c$  increases by 15%. The lower  $J_c$  in the range from 0.3 to 0.5 indicates that surface and line pinning centers poorly anchor the vortex lattice in this range of operation of point pinning centers.

Beloshenko et al. [27, 28] showed that ECMAP methods significantly increase density of surface and line pinning centers. This leads to high  $J_c$ . Results for sample B

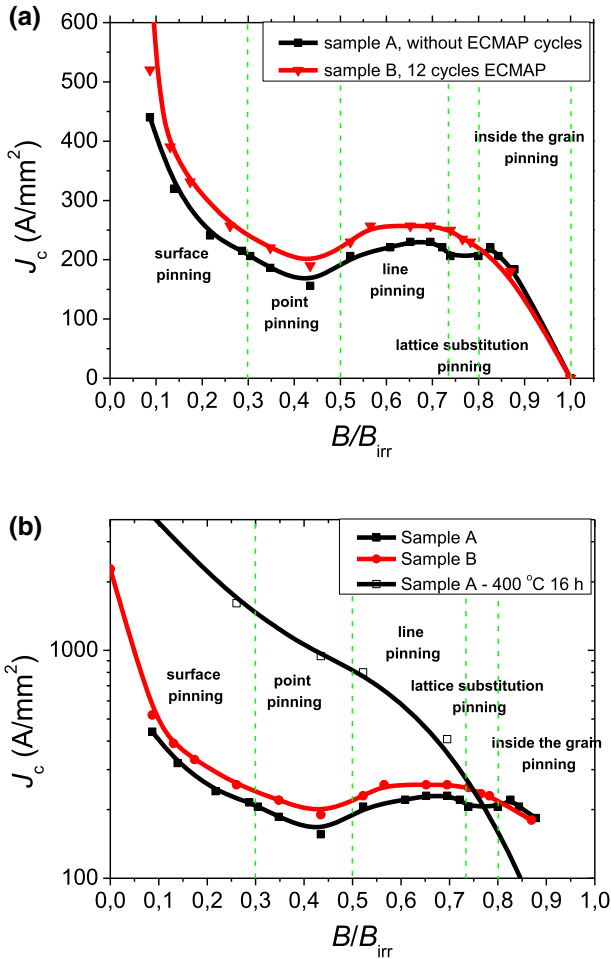


**Fig. 1** Transport  $J_c$  dependence on the reduced magnetic field ( $B/B_{irr}$ ) for NbTi wires (samples A and B): **a** without heat treatment and **b** after heat treatment at 400 °C for 16 h (Color figure online)

(Fig. 1a) show that even so, more surface and line pinning centers do not significantly increase  $J_c$  in the range from 0.3 to 0.5. These results indicate that surface pinning and line pinning cannot replace point pinning centers (precipitates with thickness close to the coherence length) because performance is poor in the magnetic field range of point pinning centers.

The results in Ref. [18] indicate that the vortex lattice in the range of  $B/B_{irr} = 0.5$ – $0.74$  is anchored by line pinning centers (dislocations) (Fig. 1a). The  $J_c$  in sample A is increased by 15% in the reduced field range from 0.5 to 0.74 and the  $J_c$  in sample B by 5% in the range from 0.5 to 0.74 compared to  $J_c$  for samples A and B in the range of 0.3–0.5. Cold drawing and ECMAP method [27, 28, 76] increase density of dislocation. This leads to an increase in  $J_c$  in the range from 0.5 to 0.74.



In the range from 0.74 to 0.8,  $J_c$  decreases by 15% in sample A and by 25% in sample B, because in these samples we do not have crystal lattice substitution pinning. Sample A has a dislocation density of about  $10^6 \text{ cm}^{-2}$  [27, 28, 76], whereas the sample B has a dislocation density of about  $10^{11} \text{ cm}^{-2}$  [27, 28, 76]. This suggests that the higher density of line pinning centers in sample B increases  $J_c$  in the range of action of lattice substitution pinning in comparison with sample A. Nevertheless, even a large number of line pinning centers can only poorly anchor the vortex lattice because in the range from 0.74 to 0.8, we see a decrease in  $J_c$  in sample B. Figure 1a shows a large reduction in  $J_c$  in the range of 0.8–1. Studies in Ref. [18] have shown that pinning centers inside grains are precipitates inside grains. These results also show that the effectiveness (anchoring of vortex lattice) of precipitates inside grains depends on their thickness [18]. On the basis of Ref. [18], it can be deduced that precipitates inside the grains with thickness close to the coherence length more effectively increase  $J_c$  in the range from 0.8 to 1 than precipitates inside the grains with thickness larger or smaller than the coherence length.

The poor increase in  $J_c$  above 0.8 T in sample B indicates that the ECMAP method does not affect the pinning centers created by Ti precipitates inside the grains. This suggests that the higher dislocation density does not affect the properties of precipitates inside the grains (better anchoring of the vortex lattice).

The Dew-Hughes [5] analysis for sample A after annealing at 400 °C for 16 h indicates that this sample has a point dominant pinning mechanism. The results show that annealing significantly increases the  $J_c$  in the range of 0–0.74 and decreases  $J_c$  above 0.74. The analysis in Fig. 1b shows that, in sample A after annealing, the  $J_c$  is decreased by 70% in the range from 0 to 0.3, by 42% from 0.3 to 0.5, by 70% from 0.5 to 0.74, by 55% from 0.74 to 0.8, and by 83% above 0.8. The annealing of the NbTi wires creates Ti precipitates between grains and removes dislocations and Ti precipitation inside grains [18]. The Ti precipitates can form point and surface pinning centers. Therefore,  $J_c$  is strongly increased in the range from 0 to 0.5. Removal of dislocations and Ti precipitation inside grains causes a significant decrease in  $J_c$  in the range from 0.5 to 0.74 and from 0.8 to 1. Comparison of  $J_c$  for samples before heating and after heating indicates, however, that  $J_c$  after heating is higher by 20–70% in the range from 0.5 to 0.74. This implies that the point pinning centers (Ti precipitates) can effectively increase  $J_c$  in the range of line pinning centers. The significant reduction in  $J_c$  above 0.74 indicates that point pinning centers are very poor at increasing  $J_c$  in high magnetic fields.

It was also shown that a higher density of dislocations increases the formation rate of precipitates between the grains in NbTi wires during heat treatment [85]. Results indicated that isostatic pressure of 0.5 GPa also increases the formation rate of Ti precipitates between the grains and slightly increases the density of high-field pinning centers [85].

These studies indicate that high  $J_c$  in NbTi wires in low and medium magnetic fields is obtained after annealing. Unfortunately, heat treatment removes high-field pinning centers, e.g., dislocations and Ti precipitates inside grains. This leads to low  $J_c$  in high magnetic fields. The studies in Ref. [18] show that pinning centers created by substitution in the crystal lattice may be the only method that can increase  $J_c$  in

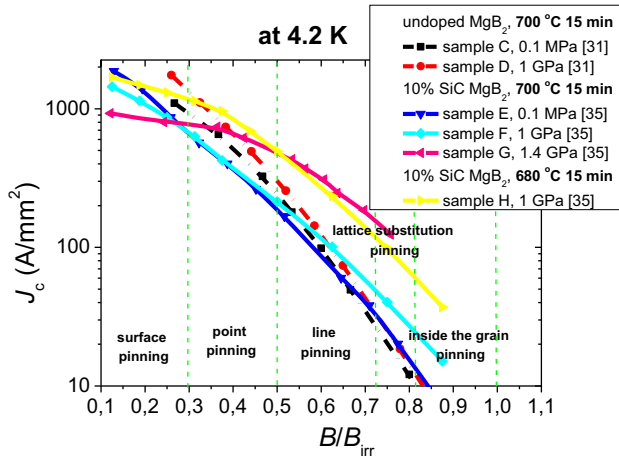


**Fig. 2** Transport  $J_c$  dependence on the reduced magnetic field ( $B/B_{irr}$ ) for undoped and doped  $MgB_2$  wires with a diameter of 0.83 mm at 4.2 K (Color figure online)

NbTi wires in high magnetic fields. These pinning centers are not removed by heat treatment.

## 6 Analysis of Pinning Centers in $MgB_2$ Wires

### 6.1 At 4.2 K

Analyzing the results for undoped  $MgB_2$  wires (samples C and D) in Fig. 2, we see that  $J_c$  decreases by 70% in the reduced field range from 0.3 to 0.5, from 0.5 to 0.74, and from 0.74 to 0.8. This indicates that, in undoped  $MgB_2$ , we have mainly surface pinning centers and a very small number of point pinning centers. The results in Fig. 2 indicate that high pressure increases  $J_c$  by 20% in the range from 0.3 to 0.8 and increases  $J_c$  by 60% below 0.3. This indicates that high pressure mainly increases the density of the surface pinning centers and the number of connections between the grains in undoped  $MgB_2$  wires. This is consistent with the results obtained by Dew-Hughes [5], which indicates that the undoped  $MgB_2$  wires have a surface dominant pinning mechanism [31]. The increase in  $J_c$  by 20% in sample D (1 GPa) suggests that high pressure increases density of point and line pinning centers.

A Si admixture in  $MgB_2$  material creates point and surface pinning centers (between the grains) [35]. On the other hand, C admixture creates lattice substitution pinning, because C substitutes for B [69]. Serquis et al. [32] demonstrated that the HIP process creates more dislocations (line pinning centers). The Dew-Hughes [5] method indicated that in samples E (0.1 MPa) and F (1 GPa) with 10% SiC we have a surface dominant pinning mechanism [35]. This analysis in Fig. 2 allows us to conduct research on other types of pinning centers. In Fig. 2, we observe that high pressure decreases  $J_c$  in sample F in comparison with sample E in the range from 0.1 to 0.3

(surface pinning). This indicates that high pressure decreases the number of surface pinning centers. This is related to the higher density of  $\text{MgB}_2$  material after the HIP process [31, 35]. Figure 2 shows that  $J_c$  does not change in the range from 0.3 to 0.5 (point pinning) in samples E and F, so high pressure does not increase the density of point pinning centers after annealing at 700 °C. Figure 2 also shows that pressure of 1 GPa increases  $J_c$  in the range from 0.5 to 0.74 (line pinning), from 0.74 to 0.8 (lattice substitution pinning), and above 0.82 (pinning inside grains). This indicates that high pressure creates high-field pinning centers in doped  $\text{MgB}_2$  wires.

In Fig. 2,  $J_c$  in sample F decreases by 70% in the range from 0.5 to 0.74 and decreases by 40% in the range from 0.74 to 0.8. This suggests that high pressure creates more lattice substitution pinning centers and indicates that the HIP process accelerates C substitution for B. Figure 2 shows that  $J_c$  in sample E (0.1 MPa) decreases by 80% in the range from 0.1 to 0.8, indicating that this sample has the most surface pinning centers.

Dew-Hughes analysis of sample G indicated that this sample has a point dominant pinning mechanism [35]. The results for samples F (1 GPa) and G (1.4 GPa) show that pressure of 1.4 GPa can significantly increase  $J_c$  above 0.3 and decreases  $J_c$  below 0.3 (Fig. 2). In sample G,  $J_c$  is decreased by 17% in the range from 0.1 to 0.3. Results for  $\text{MgB}_2$  wires (samples C, D, E, and F) and NbTi wires (samples A and B) show that the surface pinning centers significantly reduce  $J_c$  in the range from 0.1 to 0.3. Therefore, the small reduction in  $J_c$  indicates that sample G has a very small number of surface pinning centers. Figure 2 shows that point pinning centers cannot replace surface pinning centers because the  $J_c$  in sample G is lower than the  $J_c$  in sample F (surface pinning centers). In the range from 0.3 to 0.5, we see that  $J_c$  in sample G decreases by 30%. This suggests that there are a large number of point pinning centers in sample G. These pinning centers are precipitates between grains with sizes close to the coherence length. On the other hand, in the range from 0.5 to 0.74 and above 0.74 we observe a decrease in  $J_c$  of 65%. Results for NbTi wires in Fig. 1 show that high density of dislocations slightly change  $J_c$  in the range from 0.5 to 0.74. In Fig. 1, we see significantly reduction in  $J_c$  in the range from 0.5 to 0.74 in NbTi wires in which the dominant pinning mechanism mainly forms Ti precipitation between the grains. This indicates that, in sample G, only a small number of high-field pinning centers are formed. This leads to the conclusion that only a small amount of C has substituted for B, so the extra precipitates between the grains are also C. The large increase in  $J_c$  in sample G above 0.3 in comparison with the sample F indicates that precipitates between grains with a similar size to the coherence length can also effectively increase  $J_c$  in high magnetic fields.

Dew-Hughes analysis for sample H (1 GPa and 680 °C) indicated that this sample has the point dominant pinning mechanism in the range of  $B/B_{\text{irr}} = 0\text{--}0.4$  and the surface dominant pinning mechanism above 0.4 [35]. Results for samples F (1 GPa and 700 °C) and H (1 GPa and 680 °C) show that the annealing temperature of 680 °C can significantly increase  $J_c$  from 0.1 to 0.9 (Fig. 2). The results for sample H show that  $J_c$  in the range from 0.1 to 0.3 decreased by 35% and that in the range from 0.3 to 0.5 decreased by 45%. This may suggest that we have a similar number of surface and point pinning centers in sample H. In the ranges from 0.5 to 0.74 and from 0.74 to 0.8, we see a significant reduction in  $J_c$  by 80% and 65%, respectively. Based on the results

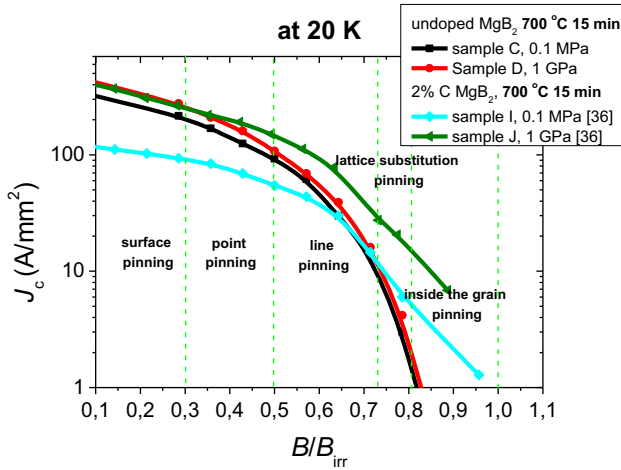


**Fig. 3** Transport  $J_c$  dependence on the reduced magnetic field  $B/B_{irr}$  for undoped and doped  $\text{MgB}_2$  wires with a diameter of 0.83 mm at 20 K (Color figure online)

for NbTi wires and  $\text{MgB}_2$  wire (sample G), we can conclude that, in sample H, we have a very small amount of high-field pinning centers. This leads to the conclusion that only a small amount of C has substituted for B and that the precipitates between the grains are also C. The results for samples H and G show that point pinning centers (precipitates between grains) also effectively increase the  $J_c$  in high magnetic fields.

By comparison of samples C (undoped and 0.1 MPa), E (10% SiC and 0.1 MPa), D (undoped and 1 GPa), and F (10% SiC and 1 GPa) F, we see that doping increases  $J_c$  above  $B/B_{irr}$  of 0.65 and decreases  $J_c$  below 0.65 (Fig. 2). This indicates that the doping creates high-field pinning centers and decreases the number of surface pinning centers. The larger increase in  $J_c$  in sample F than sample E above 0.65 indicates that the HIP process can increase the density of high-field pinning centers and accelerate the substitution of C for B (Fig. 2).

## 6.2 At 20 K

Dew-Hughes analysis at 20 K of samples C and D shows that, in the range of  $B/B_{irr} = 0-0.3$ , the point pinning mechanism is dominant. On the other hand, above 0.3 in samples C and D, the surface pinning mechanism is dominant. The results in Fig. 3 show that  $J_c$  in samples C and D is decreased by 50% in the ranges from 0.1 to 0.3 and from 0.3 to 0.5. This suggests that samples C and D have a similar number of surface and point pinning centers. On the other hand,  $J_c$  in samples C and D is reduced by one order of magnitude in the ranges from 0.5 to 0.74 and from 0.74 to 0.8 (Fig. 3). This indicates that samples C and D have only a small number of high-field pinning centers.

Dew-Hughes analysis at 20 K of samples I and J shows that, in the range from 0 to 0.65, the point pinning mechanism is dominant [36]. On the other hand, above 0.65 in samples I and J, the surface pinning mechanism is dominant [36]. The results in Fig. 3

show that  $J_c$  in samples I and J is decreased by 20% in the range from 0.1 to 0.3, by 35% in the range from 0.3 to 0.5, by 80% in the range from 0.5 to 0.74, and by 50% in the range from 0.74 to 0.8. This suggests that samples I and J mainly have point. It also indicates that the samples I and J have only a small number of surface and line pinning centers.

The results for sample C (undoped, 0.1 MPa) and sample I (2% C, 0.1 MPa) show that C doping and low pressure can increase  $J_c$  by 30% in the range from 0.72 to 0.8 (lattice substitution pinning). This means that C doping and low pressure create high-field pinning centers.

At 20 K, the measurement results for sample D (undoped, 1 GPa) and sample J (2% C, 1 GPa) show that C doping and high pressure can slightly increase  $J_c$  from 0.3 to 0.5 (Fig. 3). On the other hand, C doping and high pressure increase  $J_c$  by 35% in the range from 0.5 to 0.74 and by 75% in the range from 0.74 to 0.8. The greatest increase in  $J_c$  in the range from 0.74 to 0.8 indicates that high pressure accelerates the substitution of C for B and creates more crystal lattice substitution pinning. In addition, the research indicates that the HIP process also creates point and line pinning centers in C-doped  $MgB_2$  wires.

Annealing of the in situ undoped  $MgB_2$  material leads to the shrinking of  $MgB_2$ . The shrinking of  $MgB_2$  creates voids and strains. These big voids create low-field pinning centers (surface pinning centers) in the  $MgB_2$  material [25]. In contrast, strains create defects inside the grains. These defects form high-fields pinning centers. Jie et al. [88] showed that the use of high pressure and C encapsulated boron leads to a greater number of high-field pinning centers. Research has shown that impurities reduce the density of high-field pinning centers [25, 89].

## 7 Discussion and Conclusions

High-field pinning centers are very important in superconducting wires, because they allow us to significantly increase  $J_{ct}$  and  $J_{cm}$  in high magnetic fields. Currently, the most commonly used methods for the analysis of the dominant pinning mechanism are those of D. Dew-Hughes [5] and Higuchi et al. [6]. These methods indicate the type of pinning centers that have the highest density in the superconductor material. The maximum pinning force is necessary for analyzing the dominant pinning mechanism by using the methods of D. Dew-Hughes [5] and Higuchi et al. [6]. The Dew-Hughes method [5] also requires the determination of the irreversible magnetic field ( $B_{irr}$ ) in the superconducting wire. The  $B_{irr}$  is determined by the respective criterion of 10% of the normal-state resistance [36]. The irreversible magnetic field is also determined by Kramer's analysis ( $B^{0.25} * J_c^{0.5}$ ) [4]. This method is used in superconducting materials with a high irreversible magnetic field. The value of  $B_{irr}$  is dependent on high-field pinning centers [39, 62, 70, 71]. The results in Ref. [18] show that transport measurement methods allow us to investigate low, middle, and high-field pinning centers. The results in Ref. [18] show that magnetic measurements make it possible to investigate the low-field pinning centers, middle-field pinning centers, and high-field pinning centers (substitution for the crystal lattice, stains, and pinning centers inside grains), although magnetic measurements do not detect the line pinning centers created by dis-

locations [18]. In undoped  $\text{MgB}_2$  wires,  $\text{MgB}_2$  shrinkage creates strains, which create high-fields pinning centers. Such a study should indicate that strains are in structure of  $\text{MgB}_2$  wires. This allows to correctly determine  $B_{\text{irr}}$  from the hysteresis loop for undoped  $\text{MgB}_2$  wires. A badly defined  $B_{\text{irr}}$  does not allow us to correctly determine the dominant pinning mechanism and the behavior of other types of pinning centers. With magnetic measurements, we can correctly determine the value of  $B_{\text{irr}}$  by using the Kramer analysis in doped wires and doped bulks. Such a study should indicate that a dopant creates lattice substitution pinning centers. The lack of this kind of pinning center indicates that  $B_{\text{irr}}$  is not correct. This leads to an incorrect analysis of the dominant pinning mechanism.

The results for NbTi wires and  $\text{MgB}_2$  wires show that a reduction in  $J_c$  by 80% or one order of magnitude indicates that the surface pinning centers are dominant. This also is confirmed by the Dew-Hughes [5] method. Such a large reduction in  $J_c$  in the range of 0.1–1 indicates that we have only a small number of middle- and high-field pinning centers. Reduction in  $J_c$  from 7 to 30%, e.g., in the range from 0.3 to 0.5, indicates that we have a large number of point pinning centers. The Dew-Hughes [5] and Higuchi et al. [6] methods show similar results. Reduction in  $J_c$  from 30 to 50%, e.g., in the ranges from 0.1 to 0.3 and from 0.3 to 0.5, indicates that we have a similar number of surface and point pinning centers. Therefore, Dew-Hughes [5] analysis shows that the dominant pinning mechanism changes from point pinning to surface pinning [35]. In addition, the analysis in Figs. 1, 2, and 3 shows that this method of pinning center analysis allows to observe even small changes in the density of pinning centers. This is very important because it allows to indicate which parameters of annealing treatment (time, temperature, pressure, admixture) increase the density of high-field pinning centers and which reduce the density of high-field pinning centers. This allows to optimize the process of producing superconductor wires to obtain the highest  $J_c$ .

Strong pinning centers are pinning centers which increase mostly  $J_c$  in low or medium or high magnetic fields. This indicates that strong pinning centers mean the high density of pinning centers. On the other hand, weak pinning centers determine the low density of pinning centers. The results show that the strong pinning centers in  $\text{MgB}_2$  and NbTi wires in low magnetic fields form surface pinning centers (large voids and precipitation). In addition, the research indicates that point and high-field pinning centers are weak pinning centers in low magnetic fields. The results in Figs. 1, 2, and 3 show that surface and point pinning centers are weak pinning centers in high magnetic fields in NbTi and  $\text{MgB}_2$  wires. Based on the results, we can indicate that in high magnetic fields strong pinning centers are created by dislocations, strains, substitutions of C for B, and Ti precipitation inside grain.

**Acknowledgements** The author are grateful for the help and support for the scientific research that they have received from the Institute of Low Temperature and Structure Research PAS, Wroclaw, Poland (for A.J. Zaleski), from the Institute of High Pressure Physics PAS, Warsaw, Poland (for A.J. Morawski), from Hyper Tech Research, Columbus, Ohio, USA (for M.A. Rindfleisch), and from the Institute for Superconducting and Electronic Materials, Australian Institute of Innovative Materials (AIIM), University of Wollongong, North Wollongong, Australia (for M.S.A. Hossain). The author hereby thank V. Beloshenko, N. Matrosov, V. Chishko, V. Spuskanyuk, and W. Michailow with the A. A. Galkin Donetsk Physicotechnical Institute, Donetsk, Ukraine, and V.P. Dyakonov with the Institute of Physics PAS, Warsaw, Poland, for the NbTi

wire used in this study. The authors are very grateful to M.A. Rindfleisch and T. Tomsic with Hyper Tech Research, Columbus, Ohio, USA, for the MgB<sub>2</sub> wires used in this study.

**Open Access** This article is distributed under the terms of the Creative Commons Attribution 4.0 International License (<http://creativecommons.org/licenses/by/4.0/>), which permits unrestricted use, distribution, and reproduction in any medium, provided you give appropriate credit to the original author(s) and the source, provide a link to the Creative Commons license, and indicate if changes were made.

## References

1. G. Blatter, M.V. Feigelman, V.B. Geshkenbein, A.I. Larkin, V.M. Vinokur, *Rev. Mod. Phys.* **66**, 1125 (1994)
2. J.D. Livingston, GE R&D Center report (1969–1970). [www.bnl.gov/magnets/staff/gupta/Summer1968/0377.pdf](http://www.bnl.gov/magnets/staff/gupta/Summer1968/0377.pdf)
3. E.J. Kramer, *J. Electron. Mater.* **4**, 839 (1975)
4. E.J. Kramer, *J. Appl. Phys.* **44**, 1360 (1973)
5. D. Dew-Hughes, *Philos. Mag.* **30**, 293 (1974)
6. T. Higuchi, S.I. Yoo, M. Murakami, *Phys. Rev. B* **59**, 1514 (1999)
7. J.E. Evetts, C.J.G. Plummer, in *Proceedings of International Symposium on Flux Pinning and Electromagnetic Properties in Superconductors*, Fukuoka (1985), p. 146
8. W.A. Fietz, W.W. Webb, *Phys. Rev.* **178**, 657 (1969)
9. R.G. Hampshire, M.T. Taylor, *J. Phys. F Met. Phys.* **2**, 89 (1972)
10. A.K. Key, R.G. Hampshire, *Supercond. Sci. Technol.* **16**, 1097 (2003)
11. J.W. Ekin, *Supercond. Sci. Technol.* **23**, 083001 (2010)
12. M.J. Qin, X.L. Wang, H.K. Liu, S.X. Dou, *Phys. Rev. B* **65**, 132508 (2002)
13. S.R. Ghorbani, X.L. Wang, S.X. Dou, S.I. Lee, M.S.I. Hossain, *Phys. Rev. B* **78**, 184502 (2008)
14. T. Matsushita, *Flux Pinning in Superconductors* (Springer, Berlin, 2007)
15. W.K. Kwok, U. Welp, A. Glatz, A.E. Koshelev, K.J. Kihlstrom, G. Carabtree, *Rep. Prog. Phys.* **79**, 116501 (2016)
16. A.U. Thomann, V.B. Geshkenbein, G. Blatter, *Phys. Rev. B* **96**, 144516 (2017)
17. F.C. Klaassen, G. Doornbos, J.M. Huijbregtse, R.C.F. van der Geest, B. Dam, R. Giessen, *Phys. Rev. B* **64**, 184523 (2001)
18. D. Gajda, A. Zaleski, A. Morawski, M.S.A. Hossain, *Supercond. Sci. Technol.* **30**, 085011 (2017)
19. M. Panek, D. Pattanayak, R. Meier-Hirmer, H. Kupfer, *J. Appl. Phys.* **54**, 7083 (1983)
20. T. Matsushita, H. Kupfer, *J. Appl. Phys.* **63**, 5048 (1988)
21. G. Gajda, A. Morawski, R. Diduszko, T. Cetner, M.S.A. Hossain, K. Gruszka, D. Gajda, P. Przysluski, *J. Alloys Compd.* **709**, 473–480 (2017)
22. X. Xu, S.X. Dou, X.L. Wang, J.H. Kim, J.A. Stride, M. Choucair, W.K. Yeoh, R.K. Zheng, S.P. Ringer, *Supercond. Sci. Technol.* **23**, 085003 (2010)
23. P.J. Lee, J.C. McKinnell, D.C. Larbalestier, *IEEE Trans. Appl. Supercond.* **25**, 1918 (1989)
24. C. Baker, *J. Mater. Sci.* **5**, 40 (1970)
25. D. Gajda, A. Morawski, A.J. Zaleski, W. Haßler, K. Nenkov, M.A. Rindfleisch, E. Żuchowska, G. Gajda, T. Czujko, T. Cetner, M.S.A. Hossain, *J. Appl. Phys.* **117**, 173908 (2015)
26. M.A. Susner, T.W. Daniels, M.D. Sumption, M.A. Rindfleisch, C.J. Thong, E.W. Collins, *Supercond. Sci. Technol.* **25**, 065002 (2012)
27. V.A. Beloshenko, T.E. Konstantinova, N.I. Matrosov, V.Z. Spuskanyuk, V.V. Chishko, D. Gajda, A.J. Zaleski, V.P. Dyakonov, R. Puzniak, H. Szymczak, *J. Supercond. Nov. Magn.* **22**, 505–510 (2008)
28. V.A. Beloshenko, N.I. Matrosov, V.V. Chishko, É.A. Medvedskaya, D. Gajda, A.J. Zaleski, V.P. Dyakonov, R. Puzniak, H. Szymczak, *Low Temp. Phys.* **34**, 606–609 (2008)
29. W. Haßler, M. Herrmann, C. Rodig, M. Schubert, K. Nenkov, B. Holzapfel, *Supercond. Sci. Technol.* **21**, 062001 (2008)
30. M.S.A. Hossain, C. Senatore, M. Rindfleisch, R. Flukiger, *Supercond. Sci. Technol.* **24**, 075013 (2011)
31. D. Gajda, A. Morawski, A. Zaleski, M. Kurnatowska, T. Cetner, G. Gajda, A. Presz, M. Rindfleisch, M. Tomsic, *Supercond. Sci. Technol.* **28**, 015002 (2015)

32. A. Serquis, L. Civale, D.L. Hammon, X.Z. Liao, J.Y. Coulter, Y.T. Zhu, M. Jaime, D.E. Peterson, F.M. Mueller, V.F. Nesterenko, Y. Gu, Appl. Phys. Lett. **82**, 2847 (2003)
33. B. Birajdar, O. Eibl, J. Appl. Phys. **105**, 033903 (2009)
34. Y. Liu, F. Lan, Z. Ma, N. Chen, H. Li, S. Barua, D. Patel, M.S.A. Hossain, S. Acar, J.H. Kim, S.X. Dou, Supercond. Sci. Technol. **28**, 055005 (2015)
35. D. Gajda, A. Zaleski, A. Morawski, T. Cetner, C.J. Thong, M.A. Rindfleisch, Supercond. Sci. Technol. **29**, 085010 (2016)
36. D. Gajda, A. Morawski, A.J. Zaleski, W. Häbler, K. Nenkov, M. Małecka, M.A. Rindfleisch, M.S.A. Hossain, M. Tomsic, J. Appl. Phys. **120**, 113901 (2016)
37. P.J. Lee, *Abridged Metallurgy of Ductile Alloy Superconductors*, Wiley Encyclopedia of Electrical and Electronics Engineering, vol. 24 (1999). [http://fs.magnet.fsu.edu/~lee/asc/pdf\\_papers/589.pdf](http://fs.magnet.fsu.edu/~lee/asc/pdf_papers/589.pdf)
38. L. Cooley, P.J. Lee, D.C. Larbalestier, *Processing of Low  $T_c$  Conductors*, Handbook of Superconducting Materials (Institute of Physics Publishing, Bristol, 2003), pp. 603–639
39. H. Hillmann, Supercond. Sci. Technol. **12**, 348–355 (1999)
40. I. Pfeiffer, H. Hillmann, Acta Metall. **16**, 1429–1439 (1968)
41. O.V. Chernyi, N.F. Andrievskaya, V.O. Ilicheva, G.E. Storozhilov, G.E. Lee, A.A. Squitieri, AIP Conf. Proc. **614**, 883–890 (2002)
42. O.V. Chernyi, G.F. Tikhinskij, G.E. Storozhilov, M.B. Lazareva, Y.D. Starodubov, S.I. Savchenko, L.A. Koraiea, N.F. Andrievskaya, Supercond. Sci. Technol. **4**, 318–323 (1991)
43. J.A. Parrell, P.J. Lee, D.C. Larbalestier, IEEE Trans. Appl. Supercond. **3**, 734–737 (1993)
44. P.J. Lee, D.C. Larbalestier, Acta Metall. **35**, 2523–2536 (1987)
45. A. Cremasco, P.N. Andrade, R.J. Contieri, E.S.N. Lopes, C.R.M. Afonso, R. Caram, Mater. Des. **32**, 2387–2390 (2011)
46. P.J. Lee, J.C. McKinnell, D.C. Larbalestier, Adv. Cryog. Eng. Mater. **36**, 287–294 (1990)
47. C. Meingast, P.J. Lee, D.C. Larbalestier, J. Appl. Phys. **66**, 5962–5970 (1989)
48. C. Meingast, D.C. Larbalestier, J. Appl. Phys. **66**, 5971–5983 (1989)
49. R.W. Heussner, P.J. Lee, D.C. Larbalestier, IEEE Trans. Appl. Supercond. **3**, 757–760 (1993)
50. J.F. Li, P.X. Zhang, X.H. Liu, J.S. Li, Y. Feng, S.J. Du, T.C. Wang, W.T. Liu, G. Grunblatt, C. Verwaerde, G.K. Hoang, Physica C **468**, 1840–1842 (2008)
51. L. Cooley, P.D. Jablonski, P.J. Lee, D.C. Larbalestier, Appl. Phys. Lett. **58**, 2984–2986 (1991)
52. E.H. Brandt, Phys. Lett. A **77**, 484 (1980)
53. J.C. McKinnell, Flux pinning in superconducting Nb–Ti alloys. PhD thesis (Materials Science), University of Wisconsin-Madison (1990)
54. Y. Maintain, M. Tajima, Mater. Sci. Eng. A **438–440**, 315 (2006)
55. S. Hanada, T. Yoshio, O. Izumi, Trans. Jpn. Inst. Met. **27**, 496 (1986)
56. D.L. Moffat, D.C. Larbalestier, Metall. Trans. **19A**, 2389–2397 (1988)
57. C. Bormio-Nunes, L. Ghivelder, J. Phys. Condens. Matter **20**, 465222 (2008)
58. P.J. Lee, C.M. Fischer, D.C. Larbalestier, M.T. Naus, A.A. Squitieri, R.J. Werner, P.J. Limon, G. Sabbi, A. Zlobin, E. Gregory, IEEE Trans. Appl. Supercond. **9**, 1571 (1999)
59. R.W. Heussner, C.B. Nunes, L.D. Cooley, D.C. Larbalestier, IEEE Trans. Appl. Supercond. **7**, 1142 (1997)
60. P.J. Lee, D.C. Larbalestier, P.D. Jablonski, IEEE Trans. Appl. Supercond. **5**, 1701 (1995)
61. J. Nagamatsu, N. Nakagawa, T. Muranaka, Y. Zenitani, J. Akimitsu, Nature **410**, 63 (2001)
62. K. Vinod, R.G. Abhilash Kumar, U. Syamaprasad, Supercond. Sci. Technol. **20**, R1 (2007)
63. R. Flukiger, H.L. Suo, N. Musolino, C. Beneduce, P. Toulemonde, P. Lezza, Physica C **385**, 286–305 (2003)
64. C. Buzzea, T. Yamashita, *Magnesium Diboride in Handbook of Superconducting Materials* (Institute of Physics Publishing, Bristol, 2003), pp. 1049–1075
65. W. Pickett, Nature **418**, 733–734 (2002)
66. Z.K. Liu, D.G. Schlom, Q. Li, X.X. Xi, Appl. Phys. Lett. **78**, 3678 (2001)
67. M. Mustapić, J. Horvat, M.S. Hossain, Z. Sun, Ž. Skoko, D.R.G. Mitchell, S.X. Dou, Acta Mater. **70**, 298–306 (2014)
68. A. Jung, S.I. Schlachter, B. Runtsch, B. Ringsdorf, H. Fillinger, H. Orschulko, A. Drechsler, W. Goldacker, Supercond. Sci. Technol. **23**, 095006 (2010)
69. S. Barua, M.S.A. Hossain, Z. Ma, D. Patel, M. Mustapic, M. Somer, S. Acar, I. Kokal, A. Morawski, T. Cetner, D. Gajda, S.X. Dou, Scr. Mater. **104**, 37–40 (2015)



70. D. Gajda, A. Morawski, A.J. Zaleski, M. Akdoğan, H. Yetiş, F. Karaboğa, T. Cetner, I. Belenli, J. Alloys Compd. **687**, 616–622 (2016)
71. D. Gajda, A. Morawski, A.J. Zaleski, M. Akdoğan, H. Yetiş, F. Karaboğa, T. Cetner, I. Belenli, J. Supercond. Nov. Magn. **30**, 3397–3402 (2017)
72. D. Gajda, A. Morawski, A.J. Zaleski, W. Häbler, K. Nenkov, M. Rindfleisch, T. Cetner, M. Tomsic, J. Mater. Sci. Eng. **5**, 1000244 (2016)
73. G.Z. Li, Y. Yang, M.A. Susner, M.D. Sumption, E.W. Collings, Supercond. Sci. Technol. **25**, 025001 (2012)
74. G.Z. Li, M.D. Sumption, J.B. Zwyer, M.A. Susner, M.A. Rindfleisch, C.J. Thong, M.J. Tomsic, W. Collings, Supercond. Sci. Technol. **26**, 095007 (2013)
75. J.M. Kim, S. Oh, H. Kumakura, A. Matsumoto, Y.U. Heo, K.S. Song, Y.M. Kang, M. Maeda, M. Rindfleisch, M. Tomsic, S. Choi, S.X. Dou, Adv. Mater. **23**, 4942 (2011)
76. V.A. Beloshenko, V.P. Dyakonov, V.V. Chishko, N.I. Matrosov, O.N. Mironova, D. Gajda, A.J. Zaleski, R. Puzniak, Funct. Mater. **16**, 174 (2009)
77. M. Tomsic, M. Rindfleisch, J. Yue, K. McFadden, J. Phillips, M.D. Sumption, M. Bhatia, S. Bohnenstiehl, E.W. Collings, Int. J. Appl. Ceram. Technol. **4**, 250 (2007)
78. T. Cetner, A. Morawski, D. Gajda, W. Häbler, M. Rindfleisch, M. Tomsic, A. Zaleski, T. Czujko, E. Żuchowska, P. Przysłupski, Supercond. Sci. Technol. **28**, 045009 (2015)
79. T. Cetner, A. Morawski, K. Adamczyk, M. Rindfleisch, M. Tomsic, A. Zaleski, D. Gajda, A. Presz, High Press. Res. **32**, 419–424 (2012)
80. K. Adamczyk, A. Morawski, T. Cetner, A.J. Zaleski, D. Gajda, M. Rindfleisch, M. Tomsic, R. Diduszko, A. Presz, IEEE Trans. Appl. Supercond. **22**, 6200204 (2012)
81. D. Gajda, A.J. Zaleski, A. Morawski, M. Rindfleisch, C. Thong, M. Tomsic, Supercond. Sci. Technol. **28**, 115003 (2015)
82. D. Gajda, A. Morawski, A. Zaleski, T. Cetner, M. Małecka, A. Presz, M. Rindfleisch, M. Tomsic, C.J. Thong, P. Surdacki, Supercond. Sci. Technol. **26**, 115002 (2013)
83. A. Kario, A. Morawski, B. Głowacki, T. Łada, M. Smaga, R. Diduszko, D. Kolesnikov, A. Zaleski, A. Kondrat, D. Gajda, Acta Phys. Pol. A **111**, 693–703 (2007)
84. D. Gajda, A. Morawski, A. Zaleski, M.S.A. Hossain, M. Rindfleisch, T. Cetner, J. Alloys Compd. **647**, 303–309 (2015)
85. D. Gajda, Influence of structural defects on the critical current density of NbTi and MgB<sub>2</sub> superconducting wires. PhD thesis (Electrotechnical Sciences), Lublin University of Technology (2014)
86. D. Gajda, M. Morawski, A.J. Zaleski, M.A. Rindfleisch, C. Thong, M. Tomsic, M.S.A. Hossain, T. Cetner, Mater. Lett. **160**, 81–84 (2015)
87. D. Gajda, A. Morawski, A. Zaleski, A. Yamamoto, T. Cetner, Appl. Phys. Lett. **108**, 152601 (2016)
88. H. Jie, W. Qiua, M. Billaha, M. Mustapic, D. Patel, Z. Ma, D. Gajda, A. Morawski, T. Cetner, M. Shahabuddin, E. Yanmaz, M. Rindfleisch, J.H. Kim, M.S.A. Hossain, Scr. Mater. **129**, 79–83 (2017)
89. M. Woźniak, S.C. Hopkins, D. Gajda, B.A. Glowacki, Physica C **477**, 66–73 (2012)